X-ray vibrational studies on (100)-oriented CdTe crystals as a function of the temperature (8—350 K)

R. D. Horning and J.-L. Staudenmann
Ames Laboratory, Department of Physics, Iowa State University, Ames, Iowa 50011
(Received 24 March 1986)

The integrated intensities of the $(h,0,0)$ Bragg reflections of a CdTe single-crystal wafer have been measured at 0.546 ± 0.001 Å x-ray wavelength from the white spectrum of a tungsten anode and at 1.281 81 Å (W $L\beta_1$ excitation line). Their temperature dependences have been determined between about 8 and 360 K and analyzed with the Debye and the one-particle potential models. It is shown that the (2,0,0), (6,0,0), and (10,0,0) reflections have temperature behaviors similar to those in InSb. Furthermore, the present experimental rms atomic vibrational amplitudes are significantly higher than those predicted by some lattice-dynamical calculations.

I. INTRODUCTION

The II-VI semiconducting compound cadmium telluride has attracted considerable interest because of its many potential applications as well as for its fundamental physical properties. CdTe has the zinc-blende structure (see Fig. 1) in which each Cd atom is tetrahedrally bonded to four Te atoms and vice versa. Like most of the semiconductors (e.g., the groups IV and III-V) these crystals are characterized by partly covalent and partly ionic bonds. CdTe is one of the most ionic of this class of materials (see Zanio for an extended review[1]).

When CdTe crystals are grown by Bridgman-related methods[1,2] or by the multipass traveling heater method (THM) or sublimation THM,[3] many of the CdTe physical properties are found to be modified by Te-rich inclusions and redistribution of preexisting impurities.[4] The consequences of these inherent difficulties must be understood in order to produce well-characterized large uniform single crystals. Furthermore, it is unlikely that the Te-rich inclusions have the same thermal expansion coefficient as that of the CdTe host matrix of interest; they strain the matrix, depending upon the differences between the two thermal expansion coefficients. More recently, attention on CdTe intensified because of its use as a buffer layer between various substrates and $Hg_{1-x}Cd_xTe$ epitaxial layers,[5] and semiconductor superlattices. In the latter case, CdTe is often a constituent of the modulated structure: CdTe-HgTe, ZnTe-CdTe, and MnTe-CdTe. The large lattice mismatch between CdTe and GaAs, about 14.7%, introduces stress in the composite system.[6] As a consequence of the resulting strain, such a system behaves anomalously in the sense that the magnitude change of the two lattice parameters is four times larger than those of the corresponding bulks, when the temperature is lowered from 300 to 10 K.[7]

X-ray diffraction is a powerful analytical tool for the structural characterization of epitaxial layers and superlattices, as well as for single crystals. Temperature-dependent diffraction experiments further allow for comparisons among various atomic vibration theories, including anharmonic theories. The present paper reports on x-ray diffraction studies of the first 10 $(h,0,0)$ Bragg reflections between 10 and 350 K on a (100)-oriented CdTe crystal grown by the vertical Bridgman technique.[2] Among the various semiconducting materials, there have been two similar studies: namely, that of Bilderback and Colella on InSb, a III-V compound,[8] and that of Moss *et al.* on ZnS.[9] The comparison between CdTe and InSb is particularly interesting because the two compounds are isoelectronic: All of the four different atoms are on the same row of the periodic table and adjacent to each other. Furthermore, InSb is a "perfect" crystal and, thus, requires the use of the dynamical theory of diffraction. On the other hand, CdTe is a so-called "mosaic" crystal because the Borrmann effect,[10] which can only be explained by dynamical effects, was not observed.[11] In addition, the strain produced by the Te-rich inclusions would also impede any perfect crystal behavior. Therefore, the kinematic theory of diffraction properly accounts for the integrated intensities. The emphasis of the present study is different than that of Bilderback and Colella;[8] while they were more interested in the variation with temperature of the valence electron charge-density distribution between In and Sb, we are more concerned with the shape of the potential well in which the atoms vibrate. Thus, the measured low-angle Bragg reflections about various crystallographic orientations while the present study concentrates on the (100) orientation all the way up to the (20,0,0) reflection.

II. EXPERIMENTAL

The CdTe crystal is p type and was prepared by using polishing techniques as if it were to be used as a substrate for subsequent vapor phase epitaxy deposition. It is rectangular in shape with dimensions 3 mm × 8 mm (× 1.5 mm thick). One end of the wafer was enrobed in an indium foil for thermal contact and mechanical padding purposes. Then the enrobed part was put into a simple copper clamp which was fixed onto a copper block tightly screwed onto the cold finger of a CTI Cryogenics closed

cycle refrigerator. Two Si thermometers, calibrated by Lake Shore Cryotronics, are placed at two different levels on the copper block: one near the cold finger and the second as close as possible to the sample. With one Be vacuum outershroud and two Be radiation shields, the refrigerator can operate between about 8 and 380 K. The temperature was monitored and stabilized by a DRC-81C Lake Shore temperature controller.

The $(h,0,0)$ diffracted intensities were recorded as a function of the temperature using the x-ray wavelengths of 0.546 ± 0.001 Å from the white spectrum of a tungsten anode and of 1.281 81 Å (W $L\beta_1$ line).[12] The short wavelength from the white spectrum minimizes the effects of secondary extinction in the intense reflections, which would affect the determination of the Debye temperature. The (8,0,0) and (12,0,0) reflections of CdTe were used for orientation purposes, that is, for angle optimization prior to the measurement at a given temperature. The optimizations of the (8,0,0) and (12,0,0) were done by determining the centroids of the full ϕ, χ, and ω-2θ rocking curves, respectively, with a fine collimator limiting the entrance of the Si(Li) energy-sensitive detector. The detector collimation was then fully opened for the data collection. For each reflection, the Bragg-diffracted intensities were recorded twice: once through an ω-2θ scan and the second time through an ω scan with the 2θ detector arm set at the peak height of the first ω-2θ scan. Each of the two intensity profiles was then treated as explained previously and integrated.[13] Even though incident beam fluctuations were monitored and found to be less than 1% throughout the data collection, they have been included into the data analysis. The integrated intensities were corrected for one-phonon thermal diffuse scattering according to Rouse and Cooper,[14] and Walker and Chipman.[15] The corrected intensities for the ω-2θ and ω scans were then averaged together at each temperature and this average was used in the subsequent analysis.

III. BACKGROUND

CdTe crystallizes in the zinc-blende structure as shown in Fig. 1. In this structure, two categories of reflections can be found for the $(h,0,0)$ Bragg reflections:

(i) Strong reflections where $h=4n$ in which the scattering is produced by constructive interference from all electrons. The structure factor for these reflections is $F_{hkl}=4(f_1+f_2)$, where f_1 is the atomic form factor for the cation and f_2 refers to the anion.

(ii) Weak reflections where $h=4n+2$ resulting from the fact that the cation and the anion do not have the same number of electrons, that is, $F_{hkl}=4\,|f_1-f_2|$.

Thermal vibrations smear out the atomic positions. Thus, the form factors f_i of the atoms composing the unit cell must be modified as

$$f_i\exp(-q^2\langle u_i^2\rangle/2)=f_i\exp(-M_i) \tag{1}$$

to account for the atomic vibrations. Here $\langle u_i^2\rangle$ is the time average of the square of the atomic displacement of the atom i along the direction of the reciprocal lattice vector q. $\langle u_i^2\rangle$ is a function of the atomic position (influenced by the symmetry of the surrounding atoms) and of the nature of the studied atom. The magnitude of the

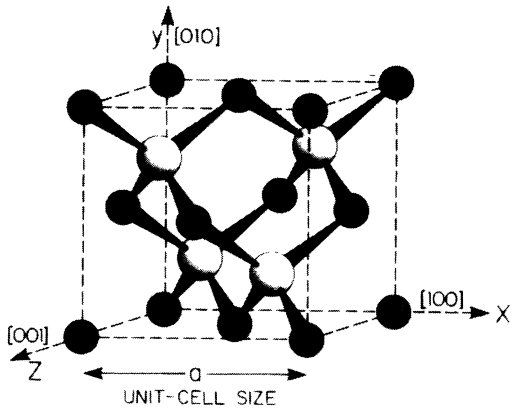

FIG. 1. Crystal structure of CdTe. It can be seen that along the [100] crystallographic axis, there are four lattice planes for one unit cell. Each (1,0,0) lattice plane is made out of only one type of atom. The CdTe lattice parameter is 6.484 Å at room temperature.

vector q is given by

$$q=4\pi(\sin\theta)/\lambda\ . \tag{2}$$

Several procedures can be used to extract vibrational information from diffraction data. The most common is to collect the structure factors of a large number of reflections at one temperature, usually room temperature. This is illustrated by Vaipolin's work[16] on CdTe at room temperature. However, no knowledge can be gained on the variations of the vibrations with temperature, or as to how well the observed behaviors fit those predicted by physical models. Measuring a complete set of reflections at a few temperatures would be far better.[9] The method used in the present article consists in measuring a few reflections at a large number of temperatures. This allows comparison with room-temperature results, as well as with various other models. This technique was applied by Walford and Schoeffel to CdTe powder samples.[17] In the case of the strong reflections, a first approximation can be made by assuming that the Cd and the Te atoms have the same $\langle u^2\rangle$. This resulting $\langle u^2\rangle$ is an average between $\langle u_{\rm Cd}^2\rangle$ and $\langle u_{\rm Te}^2\rangle$,

$$\exp(-q^2\langle u^2\rangle/2)=\sum_{i=1}^{n}f_i\exp(-q^2\langle u_i^2\rangle/2)\Big/\sum_{i=1}^{n}f_i\ , \tag{3}$$

where n is the number of different atoms in the unit cell. The square of the structure factor for those reflections becomes

$$|F_{hkl}|^2=16\,|f_{\rm Cd}+f_{\rm Te}|^2\exp(-q^2\langle u^2\rangle/2) \tag{4}$$

$$=16\,|f_{\rm Cd}+f_{\rm Te}|^2\exp(-2M)\ . \tag{4a}$$

According to the Debye theory,[18] one has

$$M=(6h^2/mk_B\Theta_M)\{0.25+\phi(x)/x\}(q/4\pi)^2\ , \tag{5}$$

where h and k_B are Planck's and Boltzmann's constants,

respectively, m is the average atomic mass of Cd and Te, θ is the Bragg angle, Θ_M is the characteristic Debye temperature, $x=\Theta_M/T$, and

$$\phi(x)=(1/x)\int_0^x [y/(\exp y-1)]dy \tag{6}$$

is the Debye function. It is common practice to exhibit the Debye temperature as a function of temperature, $\Theta_M=\Theta_M(T)$. The procedure for determining this is illustrated in Fig. 2 for the (12,0,0) reflection. The top plot is the raw data. Below it one finds a plot of $(\lambda/\sin\theta)^2\ln|F|^2$ versus the temperature. The third plot from the top represents $(\lambda/\sin\theta)^2\ln|F|^2$ as a function of $[0.25+\phi(x)/x]$. From the Debye theory,[18] the latter plot should be a straight line with a slope equal to $-12h^2/(mk_B\langle\Theta_M\rangle)$. Since $\langle\Theta_M\rangle$ is a constant, this step is only valid if $\Theta_M(T)$ is approximately constant with temperature. Therefore, a temperature range must be chosen in which it is assumed that $\Theta_M(T)$ is roughly constant. The least-squares fit is done only in this temperature range. The correct $\langle\Theta_M\rangle$ must be computed self-consistently because x is a function of $\langle\Theta_M\rangle$. The final plot of Fig. 2 shows $\Theta_M(T)$ which is deduced from the following steps.

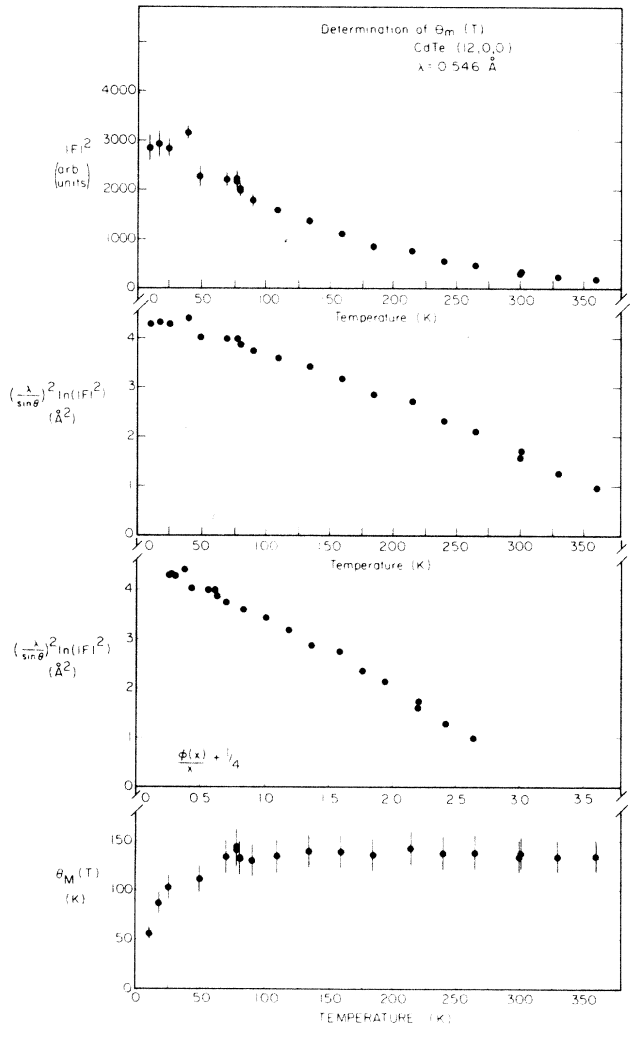

FIG. 2. Determination of the Debye temperature $\Theta_M(T)$ from the CdTe (12,0,0) Bragg reflection. The top graph is the raw data. The second is $(\lambda/\sin\theta)^2\ln|F|^2$ as a function of the temperature while the third represents the same quantity as a function of $0.25+\phi(x)/x$. According to the Debye theory, this should be, and is, a straight line. The bottom plot shows the behavior of $\Theta_M(T)$. The fluctuations in $\Theta(T)$ between 70 and 180 K are not significant when the magnitude of the errors bars are considered.

(i) Choosing a reference temperature T_0 in the temperature range of the preceding step, let $\Theta_M(T_0)=\langle\Theta_M\rangle$.

(ii) The Debye temperature $\Theta_M(T,T_0)$ at every temperature is then calculated using the formula

$$\left[\frac{\lambda}{\sin\theta}\right]^2\ln\left[\frac{F(T)}{F(T_0)}\right]^2 = -\frac{12h^2}{mk_B}\left[\frac{\phi(x)}{x\Theta_M(T,T_0)}-\frac{\phi(x_0)}{x_0\langle\Theta_M\rangle}\right]. \tag{7}$$

(iii) Steps (i) and (ii) are repeated for every T_0 in the chosen temperature range.

(iv) $\Theta_M(T)$ is then taken as the average of the $\Theta_M(T,T_0)$ at each temperature T, yielding the final plot of Fig. 2. Note if $\Theta_M(T)$ is not constant in the temperature range chosen earlier, then a new temperature range must be chosen and the procedure repeated.

Plotting Θ_M as a function of T allows one to get information beyond the temperature range in which Θ_M is constant.

Another model is the one-particle potential (OPP) model. Each atom is assumed to vibrate independently in its own potential well. Let u_1, u_2, and u_3 be the Cartesian components of the atomic displacement from equilibrium. The total displacement is given by $u^2=u_1^2+u_2^2+u_3^2$. The potential for an atom at a site of $\bar{4}3m$ point symmetry can be described by

$$V=V_0+\alpha u^2/2+\beta u_1u_2u_3+\gamma u^4 +\delta(u_1^4+u_2^4+u_3^4-3u^4/5)+\cdots, \tag{8}$$

where α, β, γ, and δ are different for each atom. The harmonic model is obtained by setting $\beta=\gamma=\delta=0$ in Eq. (8). Anharmonic effects can now be studied. β is the cubic anharmonic coefficient. γ and δ are the isotropic and anisotropic quartic anharmonic coefficients, respectively. Anharmonic refinements have been done on other compounds having the zinc-blende structure.[9,19,20] Anharmonicity is most sensitive in the $\langle 111\rangle$ directions (between nearest-neighbor atoms), while it is not as important along the [100] axis which has been probed in this experiment. Furthermore, isotropic γ and anisotropic δ quartic terms cannot be distinguished from each other when only $(h,0,0)$ reflections are considered. The temperature factor associated with the potential of Eq. (8) was first derived by Willis,[21] and later modified by Mair *et al.*[22] to include second-order terms in β which sometimes can be of the same order of magnitude as first order terms in γ and δ. The result is

$$e^{-M}=Ne^{-q^2k_BT/2\alpha}[1-k_BT(15\gamma/\alpha^2-\beta^2/2\alpha^3)+i(k_BT)^2(2\pi/a)^3(\beta/\alpha^3)hkl$$
$$+(k_BT)^2(2\pi/a)^2(10\gamma/\alpha^3-\beta^2/2\alpha^4)(h^2+k^2+l^2)$$
$$-(k_BT)^3(2\pi/a)^4(\gamma/\alpha^4)\,|\,h^2+k^2+l^2\,|^2$$
$$-0.4(k_BT)^3(2\pi/a)^4(\delta/\alpha^4)\,|\,h^4+k^4+l^4-3(h^2k^2+k^2l^2+l^2h^2)\,|$$
$$+(k_BT)^3(2\pi/a)^4(\beta^2/2\alpha^5)\,|\,h^2k^2+k^2l^2+l^2h^2\,|\,], \tag{9}$$

where

$$N=[1-k_BT(15\gamma/\alpha^2-\beta^2/2\alpha^3)]^{-1},$$

and a is the lattice parameter. For $(h,0,0)$ reflections, Eq. (9) reduces to

$$e^{-M}=Ne^{-q^2k_BT/2\alpha}[1-k_BT(15\gamma/\alpha^2-\beta^2/2\alpha^3)+(k_BT)^2(2\pi/a)^2(10\gamma/\alpha^3-\beta^2/2\alpha^4)h^2$$
$$-(k_BT)^3(2\pi/a)^4(\gamma/\alpha^4+2\delta/5\alpha^4)h^4]. \tag{9a}$$

As a consequence of the fact that the Debye temperature is very low (139 K, see below), the x-ray reflection intensities have already decayed considerably when temperatures are high enough for the anharmonic terms to become significant. In order to get meaningful results, the following simplifications are made: (1) the second-order terms in β are discarded; (2) the anisotropic quartic coefficient δ is also ignored since it is less important than γ. So Eq. (9a) is finally reduced to

$$e^{-M}=Ne^{-q^2k_BT/2\alpha}[1-15k_BT(\gamma/\alpha^2)+10(k_BT)^2(2\pi/a)^2(\gamma/\alpha^3)h^2-(k_BT)^3(2\pi/a)^4(\gamma/\alpha^4)h^4]. \tag{9b}$$

It is important to bear in mind the fact that the "γ" obtained from a least-squares fit of Eq. (9b) is really some combination of the actual β, γ, and δ. However, the effect that the real β, γ, and δ have on the shape of the potential well along the [100] axis is the same as that of the fitted γ.

IV. RESULTS

Figures 3 and 4 show the square of the observed structure factors in the form $\ln|F_{hkl}|^2$ as a function of the sample temperature. The $|F_{hkl}|^2$ were computed as $I_{hkl}/LP_2\lambda^3$, where I_{hkl} is the measured integrated intensity for the (h,k,l) reflection, L is the Lorentz factor, P_2 is the polarization factor for a mosaic crystal,[13] and λ is the x-ray wavelength. A comparison between the behaviors of the reflections in Fig. 3 and those in Fig. 4 shows a striking difference: The reflections in Fig. 3 are of the first type, while those in Fig. 4 are of the second kind (see Sec. III).

The temperature range used for all our Debye temperature calculations is $T\geq 70$ K except in the case of the (4,0,0) reflection where the domain had to be $T\geq 135$ K. The results are given in Table I. Aside from the (4,0,0) reflection, all of the Debye temperatures agree to within the uncertainty. These results are in excellent agreement with the powder work of Walford and Schoeffel.[17] Based upon the average $\langle\Theta_M\rangle=(139\pm2)$ K, the root-mean-square (rms) displacement $\langle u^2\rangle^{1/2}$ of the atoms along the [100] direction can be calculated with the relation

$$\langle u^2\rangle=(3h^2/4\pi^2mk_B\langle\Theta_M\rangle)[0.25+\phi(x)/x]. \tag{10}$$

The results are tabulated in Table II.

Three different corrections can be made to account for various physical effects which bias the diffraction data. They are all based on the fact that the Bragg angle changes slightly due to thermal expansion. The first is the so-called quasiharmonic approximation which reflects the change in the phonon frequencies, and thus Θ_M, due to thermal expansion.[23] The second is the change in the value of $(\sin\theta/\lambda)^2$ in the exponent of Eq. (3). The third is the change in the atomic form factors, which are functions of the Bragg angle. The first two are largest for the high-order reflections and the third is more important for the low-order reflections. A least-squares fit based on these corrections shows that the change in $\langle\Theta_M\rangle$ is at most 0.2 K which is smaller than the uncertainty and, therefore, not significant.

The graph of $\Theta_M(T)$ from the (12,0,0) reflection is shown as the bottom plot in Fig. 2. $\Theta_M(T)$ behaviors extracted from the (8,0,0), (16,0,0), and (20,0,0) look almost identical. $\Theta_M(T)$ from the (4,0,0) has the same shape but levels off at $\sim$104 rather than 139 K. This difference cannot be attributed to secondary extinction since that would cause Θ_M to be larger than the true value. That is, the extinction correction decreases since $|F|^2$ diminishes as the temperature is increased. The $|F|^2$ reduction is then smaller than it would be if extinction were not present. Thus, the Debye temperature would be larger.

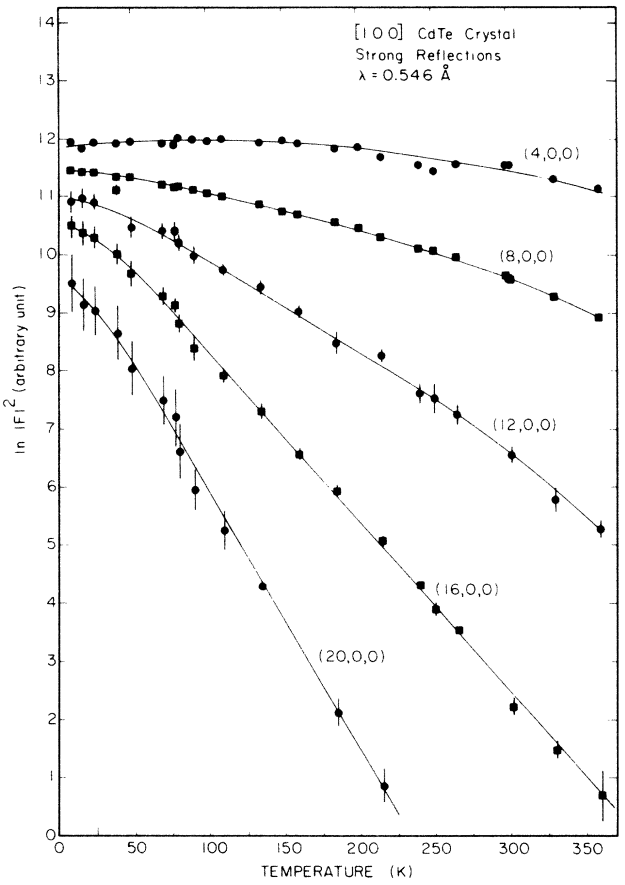

FIG. 3. Squared structure factors of the intense Bragg reflections measured as a function of the temperature. $\ln|F|^2$ is used so that all of the data sets can be shown on the same scale. These reflections exhibit typical Debye-like behaviors.

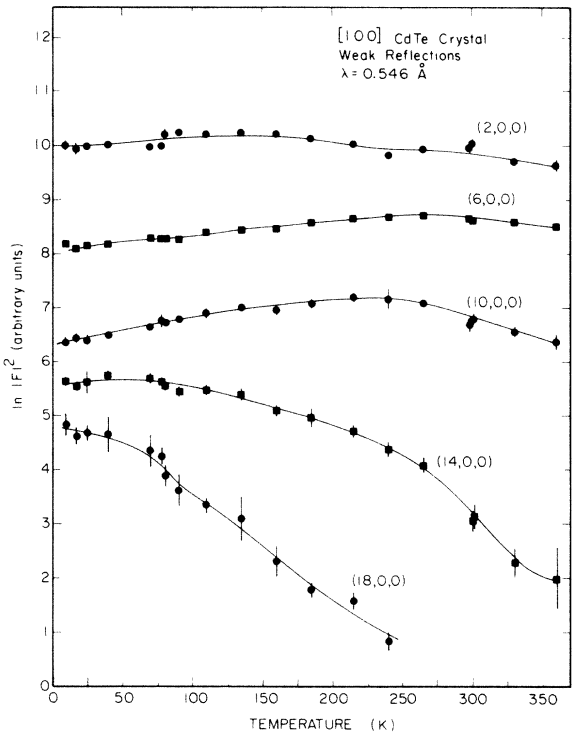

FIG. 4. Squared structure factors of the weak Bragg reflections measured as a function of the temperature. $\ln|F|^2$ is used so that all of the data sets can be shown on the same scale. These reflections, especially the (2,0,0), (6,0,0), and (10,0,0), exhibit striking non-Debye-like behaviors.

The treatment described above cannot be applied to the weak reflections. Their structure factors are

$$F_{hkl}=4[f_{\mathrm{Cd}}\exp(-M_{\mathrm{Cd}})-f_{\mathrm{Te}}\exp(-M_{\mathrm{Te}})] \quad (11)$$

and thus one cannot define an average M as could be done for the strong reflections [Eq. (3)]. In fact, Fig. 4 shows that the temperature dependence of the low-order reflections is opposite to the normal Debye-like behavior. Anomalous behavior of this sort has been observed in several other compounds having the ZnS structure, namely, InSb,[8] CuI,[24,25] CuBr,[25,26] and CuCl.[20] Since these reflections are weak, secondary extinction can be neglected. Therefore, data were also collected at an x-ray wavelength of 1.28181 Å (W $L\beta_1$ excitation line) on the (2,0,0) and (6,0,0) reflections. As seen in Fig. 5, the (2,0,0) sets of data look different from each other, but the (6,0,0) sets of data are consistent in the range $70\,\mathrm{K}\le T\le 250\,\mathrm{K}$. The (2,0,0) is strongly affected by the valence electrons because (i) it is found at small $\sin\theta/\lambda$, and (ii) the difference $|f_{\mathrm{Cd}}-f_{\mathrm{Te}}|$ is mainly a difference in the number of valence electrons of Cd and of Te, the core electrons being approximately the same in both atoms. Separating the

TABLE I. Results of the least-squares fits on the strong reflections, giving the average Debye temperature and the average α. The slope in the second column is the slope of $(\lambda/\sin\theta)^2\ln|F|^2$ as a function of $[0.25+\phi(x)/x]$.

(h,k,l)	Slope (Å^2)	$\langle\Theta_M\rangle$ (K)	α (eV/Å^2)	Temperature range
(4,0,0)	−1.84±0.07	104±4	1.05±0.01	$T\ge 135\,\mathrm{K}$
(8,0,0)	−1.383±0.006	138.5±0.6	1.362±0.004	$T\ge 70\,\mathrm{K}$
(12,0,0)	−1.40±0.03	137±3	1.351±0.001	$T\ge 70\,\mathrm{K}$
(16,0,0)	−1.37±0.02	140±2	1.412±0.005	$T\ge 70\,\mathrm{K}$
(20,0,0)	−1.35±0.07	142±7	1.49±0.08	$T\ge 70\,\mathrm{K}$
		139±2[a]	1.40±0.06[a]	

[a]Average of the four last reflections.

TABLE II. Root-mean-square atomic displacements in Å along the [100] crystallographic axis. Equation (10) is used for the Debye model while Eq. (15) is used for the OPP model. Columns 2 and 3 are the results for the "average" atom using $\langle\Theta_M\rangle=(139\pm2)$ K and $\alpha=(1.40\pm0.06)$ eV/Å^2. Columns 4 and 5 use $\langle\Theta_{M-\mathrm{Cd}}\rangle=(132\pm2)$ K and $\alpha_{\mathrm{Cd}}=(1.19\pm0.03)$ eV/Å^2, while columns 6 and 7 are calculated from $\langle\Theta_{M-\mathrm{Te}}\rangle=(143\pm1)$ K and $\alpha_{\mathrm{Te}}=(1.56\pm0.03)$ eV/Å^2, respectively. The standard deviations are about 0.002 Å for all temperatures.

	$\langle u^2\rangle^{1/2}$ (Å)		$\langle u^2_{\mathrm{Cd}}\rangle^{1/2}$ (Å)		$\langle u^2_{\mathrm{Te}}\rangle^{1/2}$ (Å)	
T (K)	Debye	OPP	Debye	OPP	Debye	OPP
70	0.070	0.066	0.076	0.071	0.066	0.063
100	0.081	0.079	0.088	0.085	0.077	0.075
150	0.098	0.096	0.107	0.104	0.093	0.092
200	0.113	0.111	0.123	0.120	0.106	0.106
250	0.126	0.124	0.137	0.135	0.119	0.118
300	0.138	0.136	0.150	0.147	0.130	0.130
350	0.148	0.147	0.162	0.159	0.140	0.140

valence effects from the vibrational effects is difficult. The (6,0,0) reflection is affected by the valence electrons to a lesser extent than the (2,0,0). The kink in the 0.546 Å (6,0,0) data at about 270 K is unexplained. A similar peculiarity is seen in the (10,0,0) data at ~250 K and less pronounced kinks are observed in the (14,0,0) and (18,0,0) at ~100 and ~75 K, respectively. For $T\geq70$ K, it is possible to explain these features by the following calculation:

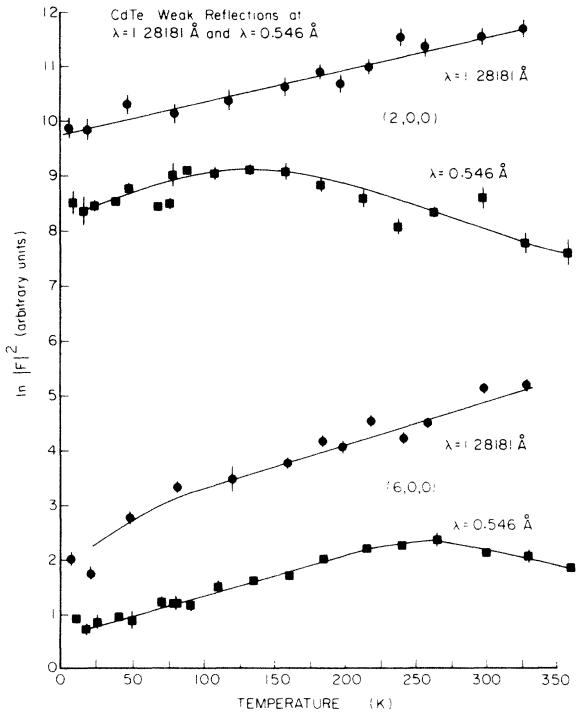

FIG. 5. Weak (2,0,0) and (6,0,0) Bragg reflections collected at the two x-ray wavelengths $\lambda=0.546$ Å and $\lambda=1.281\,81$ Å. The (2,0,0) reflections differ considerably while the (6,0,0) reflections are consistent up to about 250 K. The kink in the 0.546 Å wavelength (6,0,0) data is unexplained.

$$M=q^2\langle u^2\rangle/2\simeq UTq^2/2\ , \tag{12}$$

where U is independent of the temperature. Using this, one finds

$$|F|=|f_{\mathrm{Cd}}\exp(-U_{\mathrm{Cd}}Tq^2/2) -f_{\mathrm{Te}}\exp(-U_{\mathrm{Te}}Tq^2/2)|\ . \tag{13}$$

A positive slope in the temperature dependence, $(d|F|/dT)>0$, imposes the condition

$$(U_{\mathrm{Cd}}/U_{\mathrm{Te}})>(f_{\mathrm{Te}}/f_{\mathrm{Cd}}) \times\exp[-(U_{\mathrm{Te}}-U_{\mathrm{Cd}})Tq^2/2]\ . \tag{14}$$

Using known U's and f's, the value of T at which the slope goes to zero can be estimated. Extracting $U_{\mathrm{Cd}}=0.006\,27$ Å^2/K and $U_{\mathrm{Te}}=0.004\,57$ Å^2/K from the room-temperature data of Vaipolin,[16] and the form factors from Refs. 27(b) and 28, the temperature T_k at which the kinks are expected are listed in Table III, along with the corresponding observed values. The agreement is acceptable for all but the (6,0,0) reflection. Note again though that the kink in the (6,0,0) is not seen in the 1.281 81-Å data. Data above the kink in the (6,0,0) were not used in the following fits, and to be consistent, points in the (10,0,0) and (14,0,0) reflections were also not used above this temperature. Higher temperatures were re-

TABLE III. T_k is the temperature at which the slope of the intensity vs temperature curves for the weak reflections equal zero. The second column is calculated from Eq. (14) while the third column represents the observed values.

(h,k,l)	T_k (K) calculated	T_k (K) observed
(6,0,0)	580	270
(10,0,0)	210	250
(14,0,0)	110	100
(18,0,0)	50	75

TABLE IV. Values of the Debye temperatures extracted from the various pairs of weak and strong reflections. The standard deviations on the individual Θ_M's are on the order of 0.06 K or less, therefore they are not indicated. The pairs involving the (20,0,0) reflection give consistently high values of Θ_M, thus they are ignored in the final average. Entries with an asterisk mean that the (6,0,0) reflection was measured at 1.281 81 Å wavelength. χ^2 is the "goodness of fit" parameter which was minimized in the least squares fit.

(h,k,l) pair		Θ_{M-Cd}	Θ_{M-Te}		
Weak	Strong	(K)	(K)	R factor	χ^2
(6,0,0)	(8,0,0)	132.0	142.6	0.017	1.85
*(6,0,0)	(8,0,0)	130.1	146.0	0.040	3.65
(6,0,0)	(12,0,0)	130.7	141.2	0.017	1.54
*(6,0,0)	(12,0,0)	130.1	142.7	0.046	3.24
(6,0,0)	(16,0,0)	132.4	143.1	0.016	1.54
*(6,0,0)	(16,0,0)	131.2	143.9	0.044	3.39
(6,0,0)	(20,0,0)	135.7	146.8	0.013	1.49
*(6,0,0)	(20,0,0)	137.0	150.7	0.043	3.88
(10,0,0)	(8,0,0)	131.9	143.1	0.031	1.12
(10,0,0)	(12,0,0)	130.4	141.8	0.041	0.95
(10,0,0)	(16,0,0)	132.2	143.3	0.035	0.79
(10,0,0)	(20,0,0)	136.4	147.2	0.027	0.44
(14,0,0)	(8,0,0)	134.1	141.0	0.033	1.12
(14,0,0)	(12,0,0)	132.9	140.2	0.048	0.85
(14,0,0)	(16,0,0)	135.2	141.6	0.040	0.77
(14,0,0)	(20,0,0)	140.0	144.9	0.034	0.45
(18,0,0)	(8,0,0)	133.4	142.7	0.042	1.64
(18,0,0)	(12,0,0)	131.6	142.0	0.077	1.35
(18,0,0)	(16,0,0)	134.3	142.6	0.061	1.30
(18,0,0)	(20,0,0)	145.6	148.0	0.077	1.06
		$\langle\Theta_M\rangle = 132\pm2$,	143 ± 1		

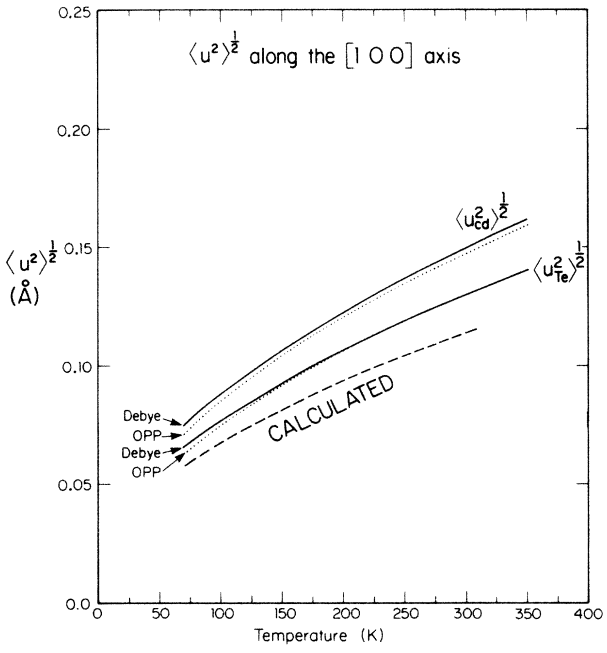

FIG. 6. Root-mean-squared atomic displacements in Å along the [100] crystallographic axis for the Cd and Te atoms as a function of the temperature. Solid lines represent the results from the Debye model using Eq. (10), $\langle\Theta_{M-Cd}\rangle = 132$ K, and $\langle\Theta_{M-Te}\rangle = 143$ K. Dotted lines are from the OPP model using Eq. (15); $\alpha_{Cd} = 1.19$ eV/Å^2, and $\alpha_{Te} = 1.56$ eV/Å^2. The dashed line is from the calculations in Ref. 32. Standard deviations are on the order of 0.002 Å or less.

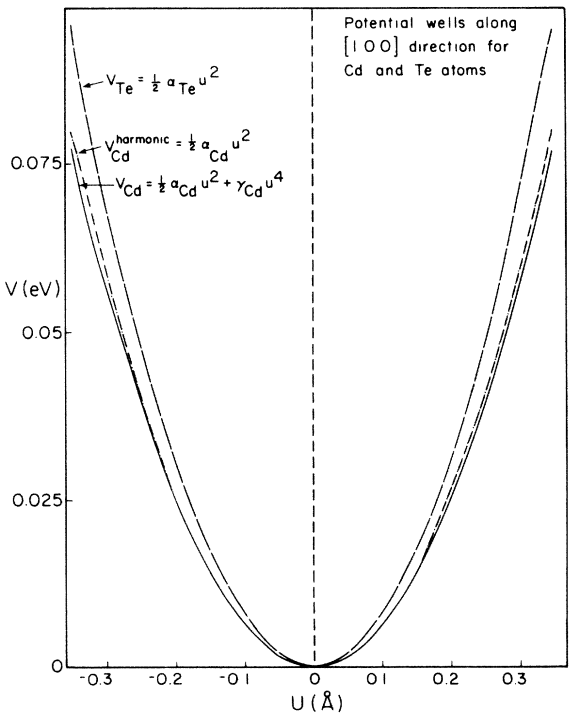

FIG. 7. Potential wells for the Cd and Te atoms as a function of atomic displacement in the [1,0,0] direction. The effect of anharmonicity on the shape of the well is shown for the Cd atom. $\alpha_{Cd} = 1.30$ eV/Å^2 and $\gamma_{Cd} = -0.21$ eV/Å^4, and $\alpha_{Te} = 1.56$ eV/Å^2.

TABLE V. Values of the coefficients α and γ in $V=V_0+\alpha u^2/2+\gamma u^4$ extracted from pairs of weak (w) and strong (s) reflections characterized only by the h Miller index. Typical standard deviations of all α's and γ's are about 0.005 or less. (i) average of all harmonic combinations except those containing the (20,0,0) reflection. (ii) Average of all anharmonic combinations except those containing the (18,0,0), (20,0,0), and the 1.281 81 Å data. (iii) average of all anharmonic combinations except those containing the (18,0,0) and (20,0,0) reflections but including the 1.281 81 Å data. (iv) average of the anharmonic combinations using only pairs marked by an asterisk in the table. The second line for each of the above cases represents the standard deviations of the various averages.

h Miller pair		Harmonic fit				Anharmonic fit				
		α_{Cd}	α_{Te}			α_{Cd}	γ_{Cd}	α_{Te}		
w	s	(eV/Å^2)		R	χ	(eV/Å^2)	(eV/Å^4)	(eV/Å^2)	R	χ
6	8	1.180	1.566	0.017	1.40	1.276	−0.184	1.564	0.016	1.29
*6	8	1.170	1.601	0.041	1.92	1.418	−0.435	1.545	0.031	1.50
6	12	1.160	1.539	0.017	1.26	1.244	−0.170	1.529	0.015	1.15
*6	12	1.148	1.569	0.046	1.81	1.386	−0.420	1.513	0.035	1.39
6	16	1.191	1.581	0.016	1.26	1.270	−0.161	1.570	0.014	1.16
*6	16	1.172	1.602	0.044	1.88	1.420	−0.425	1.555	0.033	1.46
6	20	1.268	1.689	0.013	1.20	1.313	−0.150	1.639	0.012	1.10
*6	20	1.288	1.770	0.042	1.95	1.460	−0.410	1.619	0.032	1.51
10	8	1.177	1.570	0.032	1.11	1.309	−0.235	1.551	0.030	1.04
10	12	1.155	1.545	0.043	0.95	1.275	−0.220	1.522	0.039	0.89
10	16	1.190	1.580	0.036	0.91	1.292	−0.185	1.563	0.034	0.87
10	20	1.274	1.677	0.026	0.64	1.317	−0.120	1.636	0.025	0.61
14	8	1.216	1.525	0.034	1.11	1.357	−0.267	1.506	0.032	1.05
14	12	1.200	1.510	0.050	0.94	1.329	−0.262	1.486	0.096	0.89
14	16	1.245	1.546	0.040	0.89	1.345	−0.197	1.529	0.039	0.88
14	20	1.337	1.620	0.033	0.65	1.360	−0.083	1.597	0.033	0.66
18	8	1.200	1.560	0.043	1.31	1.633	−0.886	1.498	0.031	0.99
18	12	1.172	1.551	0.078	1.17	1.617	−0.895	1.483	0.055	0.84
18	16	1.230	1.570	0.061	1.13	1.645	−0.840	1.523	0.045	0.85
18	20	1.413	1.673	0.073	0.97	1.668	−0.775	1.563	0.054	0.74
(i)		1.19	1.56							
		0.03	0.03							
(ii)						1.30	−0.21	1.54		
						0.04	0.04	0.03		
(iii)						1.33	−0.30	1.54		
						0.06	0.10	0.03		
(iv)						1.42	−0.42	1.54		
						0.04	0.01	0.02		

tained, however, in fits involving the 1.281 81 Å sets of data.

The Debye temperatures of the individual atoms can be estimated by using a pair of reflections, one strong and the other weak. A single reflection cannot be used because the correlation between Θ_{M-Cd} and Θ_{M-Te} is large in any least-squares fit. Equation (5) is still used, with m and Θ_M differing for each atom. The various fits were again done only in the temperature range from 70 to 350 K. The results for all possible pairs of strong and weak reflections are listed in Table IV where it is seen that all pairs containing the (20,0,0) reflection give unusually high Θ_M values. This is probably due to the fact that there are less measured data points for the (20,0,0) than for the others and/or because the TDS corrections used in this article ignored two-, three-, . . . , phonon scattering, which are more significant at high q's. These pairs are not included in the averages written at the end of Table IV: $\langle\Theta_{M-Cd}\rangle=(132\pm2)$ K and $\langle\Theta_{M\text{-}Te}\rangle=(143\pm1)$ K. These results agree well with those of Vaipolin[16] who reports $\Theta_{M-Cd}=134$ K and $\Theta_{M-Te}=146$ K at room temperature. Equation (10) can be used again to calculate the corresponding rms atomic displacements $\langle u^2_{Cd}\rangle^{1/2}$ and $\langle u^2_{Te}\rangle^{1/2}$ (see Table II and Fig. 6). The corrections based on thermal expansion were again checked and found to be insignificant.

Similar fits to those described above were done using the potential well model. These results are listed in Tables I and V. Based on the strong reflections, the harmonic coefficient for the average atom is $\alpha=(1.40\pm0.06)$ eV/Å^2. Pairs of reflections are further used to extract the coefficients for the individual atoms. (h,k,l) pairs including the (20,0,0) reflection were again excluded from the averages for the same reasons as above. When refining only the harmonic coefficients, the average values are $\alpha_{Cd}=(1.19\pm0.03)$ eV/Å^2 and $\alpha_{Te}=(1.56\pm0.03)$ eV/Å^2. The corresponding displacements are computed from the relation

$$\langle u^2\rangle=k_BT/\alpha\ . \tag{15}$$

These are listed in Table II and graphed as dotted lines in Fig. 6. Since the Cd atoms vibrate more than the Te

atoms, they are more sensitive to anharmonic effects. Therefore, a second set of fits was done in which the isotropic quartic coefficient γ in Eq. (9b) was included for the Cd atom only. These results are also given in Table V. The (h,k,l) pairs containing the (18,0,0) now appear to give results differing from the other pairs. This is probably due to one additional parameter being refined while there are fewer (18,0,0) data points than for the other reflections, except the (20,0,0). Excluding pairs containing either one of the two above reflections, the averages are $\alpha_{Cd}=(1.30\pm0.04)$ eV/Å^2, $\alpha_{Te}=1.54$ eV/Å^2, and $\gamma_{Cd}=(-0.21\pm0.04)$ eV/Å^4. When the (6,0,0) data taken at 1.281 81 Å wavelength is used, the harmonic fit is unaffected, but the anharmonic fit for α_{Cd} and γ_{Cd} changes the above values to (1.42 ± 0.04) eV/Å^2 and (-0.42 ± 0.01) eV/Å^4, respectively. Since higher temperatures were available in the latter case, these results might be more reliable. The negative value of γ_{Cd} indicates that the potential well for the Cd atom "softens" at large u^2. Figure 7 illustrates this well for u^2 along the [100] direction, with $\gamma_{Cd}=-0.21$ eV/Å^4.

V. DISCUSSION AND CONCLUSION

From the results of our least-squares fits, the Debye model and the OPP model can be compared. Tables IV and V show that the reliability factors (R factors) for the Debye and the harmonic OPP models are almost identical, indicating that for temperatures greater than $\sim$70 K, the two models are basically equivalent. More importantly, Fig. 6 shows the rms displacements for the Debye and the harmonic OPP models plotted together as a function of the temperature. The agreement for tellurium is almost perfect except in the low-temperature region. In the high-temperature region for Cd ($T>\langle\Theta_{M-Cd}\rangle$), the OPP result is consistently $\sim$1.7% lower than that given by the Debye result. This indicates that the fits give slightly different results, but they are still within one standard deviation of each other. However, at lower temperatures, the deviation becomes larger. In both cases, this is due to the fact that the temperature factor in the OPP model, Eq. (9), is derived in the classical, or high-temperature limit, $T>\Theta_M$. The zero-point motion is therefore neglected. In this limit, the two models are the same. The deviation for temperatures below Θ_M amounts to about 5% at 70 K which is approximately $\Theta_M/2$. This result is in good agreement with the theoretical conclusions of Mair and Wilkins[29] who use quantum statistics to extend the OPP result to lower temperatures. They also showed that the Debye and OPP models again diverge below $\sim\Theta_M/4$. Thus, little would be gained by fitting our data to the more complicated quantum OPP equation. The R-factor significance test[27a] was used to determine if the R-factor improvement found in the anharmonic fits is statistically significant. In all cases except two [both involving the (20,0,0) reflection], the improvement is significant with a confidence level greater than 90%; that is, we can be more than 90% confident that the anharmonic picture is physically more realistic than the purely harmonic model. It must be pointed out, though, that this anharmonicity is actually some combination of the isotropic and anisotropic terms. In order to resolve these anharmonic terms, further work is in progress at higher temperatures on the $(h,0,0)$-type reflections, and also on the (h,h,h) and $(h,h,0)$ families of Bragg reflections.

Calculations of the temperature factors of zinc-blende crystals using lattice dynamics were first done by Authier[30] with limited success. The more advanced rigid-ion model (RIM) (Ref. 31) and modified RIM (Ref. 32) have been used more recently. The lowest curve in Fig. 6 shows the results using the modified RIM. The Cd and Te atoms have nearly the same rms displacements. The calculation for the Te atom is 12% less than the experimental result, and 24% too low for Cd. This model apparently does not fit the inelastic neutron scattering data either.[1] Similar calculations were not available for the RIM which gives a better fit to the neutron data.

Among the experimental results presented in this paper, the most astonishing ones are those related to the temperature behaviors of the $(2n,0,0)$ reflections with $n=1,3,5,\ldots$. These effects seem smaller for the CdTe (2,0,0) than for the InSb (2,0,0) measured by Bilderback and Colella.[8] However, the magnitude change is larger in the CdTe (6,0,0) than in the corresponding InSb reflection. Since Cd, In, Sb, and Te have nearly the same electron cores, the above reflections are therefore very sensitive to physical effects such as charge transfers at low angles and to anharmonic vibrations at high angles. As shown in Fig. 1, the behaviors mentioned above take place between In and Sb atomic planes on one hand, and between Cd and Te planes, on the other. Consequently, the above comparison indicates that vibrational effects are stronger in CdTe than in InSb. In this respect, it would be interesting to confirm our thermal diffuse scattering calculations with a direct measurement of the inelastic diffracted photons, or better, to separate out the inelastic part from the total scattering by resonant γ-ray diffraction.[33]

It is instructive to extend this comparison to the I-VII compound AgI which is isoelectronic with CdTe and InSb. From the results of this paper, it is seen that the potential well in which the Cd atom moves is shallower and broader than that for the Te atom. Apparently, but to a lesser extent, this fact is also true for InSb. Since the Cd-Te bond is partly ionic, there is a transfer of some charge from Cd toward Te. The electronic configuration of Cd approaches that of the noble metal Ag, while the Te electronic configuration resembles that of iodine. It is interesting to note that the metastable γ phase of AgI has the zinc-blende structure but at higher temperatures undergoes a phase transition to a "superionic" phase;[34] the I atoms form a bcc lattice while the Ag sublattice "melts" and the silver atoms are free to move about. Undoubtedly, the Ag atoms in the γ phase have broad, shallow potential wells, and large vibration amplitudes, as a precursor to the superionic phase. Further work on the higher-order reflections of InSb and on AgI would be beneficial. Due to the many similarities, it would be worthwhile to carry out the same type of study on the isoelectronic series Ge—GaAs—ZnSe—CuBr. All of these compounds have the zinc-blende structure and, furthermore, CuBr has a superionic phase at high temperatures.

ACKNOWLEDGMENTS

The authors wish to express their appreciation to Dr. J. L. Schmit for providing the excellent CdTe crystal, Dr. D. K. Arch for many interesting comments on the physics of CdTe, to Dr. W. B. Yelon of the University of Missouri Research Reactor (MURR) for stimulating discussions on inelastic γ-ray scattering and its potential use for CdTe, and Dr. R. Triboulet of Centre National de la Recherche Scientifique (C.N.R.S.) at Meudon (France) for pointing out the many problems related to the physical stability of CdTe crystals. Ames Laboratory is operated for the U.S. Department of Energy by Iowa State University under contract No. W-7405-Eng-82. This work was supported by the Director for Energy Research, Office of Basic Energy Sciences, U.S. Department of Energy.

[1]K. Zanio, *Cadmium Telluride,* Vol. 13 of *Semiconductors and Semimetals,* edited by R. K. Willardson and A. C. Beer (Academic, New York, 1978).

[2]R. Betsch and J. L. Schmit, (private communication).

[3]R. Triboulet, J. Crys. Growth **51**, 89 (1981).

[4]J.-L. Pautrat, N. Magnea, and J.-P. Faurie, J. Appl. Phys. **53**, 8668 (1982).

[5]G. S. Almasi and A. C. Smith, J. Appl. Phys. **39**, 233 (1968); R. Dornhaus and G. Nimitz, *The Properties and Applications of the $Hg_{1-x}Cd_xTe$ Alloy System, of Solid State Physics* (Springer, Berlin, 1976), pp. 1—119, and references therein; P. W. Kruse, *The Emergence of $Hg_{1-x}Cd_xTe$ as a Modern Infrared Sensitive Material,* Vol. 18 of *Semiconductors and Semimetals* (Academic, New York, 1981), pp. 1—20.

[6]D. K. Arch, J. L. Schmit, R. D. Horning, and J.-L. Staudenmann, J. Crys. Growth **71**, 149 (1985).

[7]J.-L. Staudenmann, R. D. Horning, R. D. Knox, D. K. Arch, and J. L. Schmit, Appl. Phys. Lett. **48**, 994 (1986).

[8]D. H. Bilderback and R. Colella, Phys. Rev. B **13**, 2479 (1976); R. Colella, Phys. Scr. **15**, 143 (1977).

[9]B. Moss, R. K. McMullan, and T. F. Koetzle, J. Chem. Phys. **73**, 495 (1980).

[10]G. Borrmann, Phys. Z. **43**, 157 (1941); **127**, 297 (1950).

[11]R. D. Horning (unpublished).

[12]J.-L. Staudenmann, M. Sandholm, L. D. Chapman, and G. L. Liedl, Nucl. Instrum. Methods **222**, 177 (1984).

[13]J.-L. Staudenmann, L. D. Chapman, W. J. Murphy, R. D. Horning, and G. L. Liedl, J. Appl. Crystallogr. **18**, 519 (1985).

[14]K. D. Rouse and M. J. Cooper, Atomic Energy Research Establishment Report No. R5725 (unpublished); M. J. Cooper and K. D. Rouse, Acta Crystallogr. A **24**, 405 (1968).

[15]C. B. Walker and D. R. Chipman, Acta Crystallogr. A **25**, 395 (1969).

[16]A. A. Vaipolin, Fiz. Tverd. Tela (Leningrad) **15**, 1223 (1973) [Sov. Phys.—Solid State **15**, 823 (1973)].

[17]L. K. Walford and J. A. Schoeffel, Philos. Mag. **21**, 375 (1970).

[18]R. W. James, *The Optical Principles of the Diffraction of X-Rays* (Ox Bow Press, Connecticut, 1982).

[19]M. J. Cooper, K. D. Rouse, and H. Fuess, Acta Crystallogr. A **29**, 49 (1973); V. Valvoda and J. Jecny, Phys. Status Solidi A **45**, 269 (1978); G. McIntyre, B. Moss, and Z. Barnea, Acta Crystallogr. A **36**, 482 (1980).

[20]M. Sakata, S. Hoshino, and J. Harada, Acta Crystallogr. A **30**, 655 (1974).

[21]B. T. M. Willis, Acta Crystallogr. A **25**, 277 (1969).

[22]S. L. Mair, Z. Barnea, M. J. Cooper, and K. D. Rouse, Acta Crystallogr. A **30**, 806 (1974).

[23]B. T. M. Wilis and A. W. Pryor, *Thermal Vibrations in Crystallogrphy* (Cambridge University, Cambridge, England, 1975), pp. 142—143.

[24]S. Miyake, S. Hoshino, and T. Takenata, J. Phys. Soc. Jpn. **7**, 19 (1952).

[25]S. Miyake and S. Hoshino, Rev. Mod. Phys. **30**, 172 (1958).

[26]S. Hoshino, J. Phys. Soc. Jpn. **7**, 560 (1952).

[27](a) W. C. Hamilton, Acta Crystallogr. **18**, 502 (1965); (b) *International Tables for X-Ray Crystallography,* edited by J. A. Ibers and W. C. Hamilton, published for the International Union of Crystallography (Kynoch Press, Birmingham, England, 1974), Vol. 4.

[28]Don T. Cromer, J. Appl. Crystallogr. **16**, 437 (1983).

[29]S. L. Mair and S. W. Wilkins, J. Phys. C **9**, 1145 (1976).

[30]A. Authier, Acta Crystallogr. **9**, 411 (1956).

[31]P. Plumelle and M. Vandevyver, Phys. Status Solidi B **73**, 271 (1976).

[32]J. F. Vetelino, S. P. Gaur, and S. S. Mitra, Phys. Rev. B **5**, 2360 (1972).

[33]W. B. Yelon, *Applications of Elastic and Near Elastic γ-Ray Scattering* (Materials Research Science, Trans. Tech., Aedermannsdorf, Switzerland, 1984), pp. 81—98.

[34]W. A. Harrison, *Electronic Structure and the Properties of Solids* (Freeman, San Francisco, 1980), p. 316.

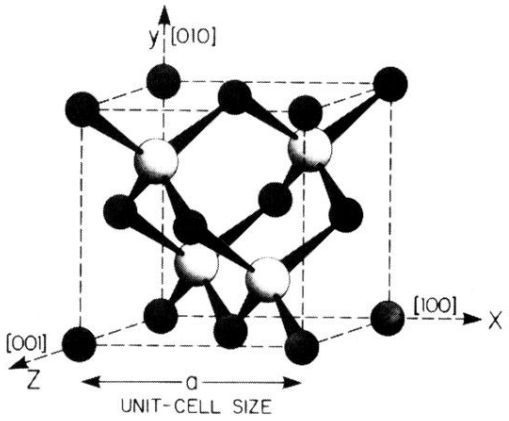

FIG. 1. Crystal structure of CdTe. It can be seen that along the [100] crystallographic axis, there are four lattice planes for one unit cell. Each (1,0,0) lattice plane is made out of only one type of atom. The CdTe lattice parameter is 6.484 Å at room temperature.